PHYSICAL REVIEW B **94**, 161201(R) (2016)

# Limit of $zT$ enhancement in rocksalt structured chalcogenides by band convergence

Min Hong,[1] Zhi-Gang Chen,[1,*] Yanzhong Pei,[2] Lei Yang,[1] and Jin Zou[1,3,†]
[1]*Materials Engineering, University of Queensland, Brisbane, Queensland 4072, Australia*
[2]*School of Materials Science and Engineering, Tongji University, Shanghai 201804, China*
[3]*Centre for Microscopy and Microanalysis, University of Queensland, Brisbane, Queensland 4072, Australia*
(Received 29 June 2016; revised manuscript received 2 September 2016; published 14 October 2016)

Rocksalt structured chalcogenides, such as PbTe, PbSe, and SnTe, are the top candidates for midtemperature thermoelectric applications, and their $p$-type thermoelectric efficiencies can be enhanced via aligning the valence bands. Here, we provided comprehensive numerical investigations on the effects of band convergence on electronic properties. We found that the extra valance band can indeed significantly enhance the power factor. Nevertheless, the extra valance band can also increase the electronic thermal conductivity, which partially offsets the enhanced power factor for the overall figure of merit. Finally, we predicted that the maximum figure of merit for PbTe, PbSe, and SnTe can reach 2.2, 1.8, and 1.6, respectively, without relying on the reduction in lattice thermal conductivity.

DOI: 10.1103/PhysRevB.94.161201

Thermoelectricity enables the direct conversion between heat and electricity, offering a sustainable green energy technique for power generation or refrigeration [1,2]. To realize wide applications, extensive strategies have been applied to enhance the conversion efficiency, gauged by the figure of merit ($zT$), which can be expressed as $zT = S^2\sigma T/k$, where $S$, $\sigma$, $\kappa$, and $T$ are the Seebeck coefficient, electrical conductivity, thermal conductivity (including electronic $\kappa_e$, lattice $\kappa_l$, and bipolar $\kappa_{bi}$ components), and the working temperature, respectively [3]. Among them, band engineering is widely used to tune the electronic band structures to pursue high power factor ($S^2\sigma$) [4–6], and other use is to enhance phonon scatterings to reduce $\kappa$ by involving different phonon scattering mechanisms [7,8].

As dominating candidates working at midtemperature range, extensive attention has been paid to rocksalt structured chalcogenides, such as PbTe, PbSe, and SnT [9–13]. They share similar band structures, in which two extrema at the $L$ ($E_{VL}$) and $\Sigma$ ($E_{V\Sigma}$) points of the Brillouin zone are separated by an energy bias ($\Delta E = E_{VL} - E_{V\Sigma}$), which is comparable to the band gap ($E_g = E_C - E_{VL}$, with $E_C$ denoting the extreme of the conduction band) [14]. Since the $\Sigma$ valance band ($VB_\Sigma$) locates further away from the Fermi level ($E_f$) compared with the $L$ valance band ($VB_L$), the $S$ tensor of $VB_\Sigma$ is larger than that of $VB_L$ [15–17]. Besides, the $VB_\Sigma$ band degeneracy ($N_\Sigma$) of rocksalt structured chalcogenides is 12, much larger than that of $VB_L$($N_L = 4$) [18]. In this regard, producing the convergence of $VB_L$ and $VB_\Sigma$ (i.e., reducing $\Delta E$) may greatly enhance the thermoelectric performance, when doping is properly tuned. Experimentally, forming $PbTe_{1-x}Se_x$ alloys can align $VB_L$ and $VB_\Sigma$, which leads to $zT$ up to 1.8 [19,20]. Sr doping was employed to reduce the $\Delta E$ for PbSe [21]. On the other hand, Mn [22,23], Cd [24,25], and Hg [12] were successfully used to reduce the $\Delta E$ for SnTe. In both PbSe and SnTe with reduced $\Delta E$, $zT$ values were significantly enhanced.

Despite these great achievements, there still exist several theoretical issues that need to be fully examined. First, the band convergence temperature ($T_{cvg}$) for achieving the maximum $zT$ has not been clarified. For example, PbTe with $T_{cvg}$ of ~450 K [21], both alloying with Se to increase $T_{cvg}$ [19,20] and doping with Mn to decrease $T_{cvg}$ [13,26], can increase $S^2\sigma$. Second, enlarging the contribution from $VB_\Sigma$ can increase $\kappa$. On one hand, enlarging the contribution from $VB_\Sigma$ leads to large $\sigma$, thereby inevitably increasing $\kappa_e$. On the other hand, additional heat flow is simultaneously generated during the electron transition between $VB_L$ and $VB_\Sigma$ [27]. Last but not least, the determination of optimal Hall carrier concentration ($n_H^{opt}$) for maximizing $S^2\sigma$ and $zT$ is in great demand for achieving the maximum thermoelectric efficiency in multiband situations [4,21].

In this study, we employed a three-band (CB, $VB_L$, and $VB_\Sigma$) model to numerically investigate the impact of band convergence on tailoring thermoelectric performance for rocksalt structured chalcogenides. Detailed equations for calculating thermoelectric properties are presented in the Supplemental Material [28], including the tensors of CB (with subscript of $C$), $VB_L$ (with subscript of $L$), and $VB_\Sigma$ (with subscript of $\Sigma$). Parameters used in our calculations are listed in Table SI [28]. On this basis, we simulated the variations of thermoelectric properties with reduced Fermi level ($\eta$) for SnTe, as an example, over a wide temperature range. We found that for maximizing $S^2\sigma$ and therefore $zT$, $T_{cvg}$ should equal the highest working temperature, which is about 900 K for SnTe, PbTe, and PbSe. Through producing band convergence to enhance $S^2\sigma$, $\kappa$ is also increased, which partially offsets the enhancement in $S^2\sigma$ for the overall $zT$. In addition, we investigated $n_H$ dependent thermoelectric properties and determined the temperature-dependent $n_H^{opt}$ values for $S^2\sigma$ and $zT$ in PbTe, PbSe, and SnTe, respectively. Using the reported $\kappa_l$ values for these rocksalt structured chalcogenides from the literature [10,14,29], we predicted the maximum $zT$ to be 2.2, 1.8, and 1.6 for PbTe, PbSe, and SnTe, respectively. If the $\kappa_l$ reaches the amorphous limit, $zT$ can be further enhanced to 3.1, 2.4, and 2.2 for PbTe, PbSe, and SnTe, respectively. This study suggests that there is plenty room for the $zT$ enhancement in these rocksalt structured chalcogenides by producing band convergence at 900 K and appropriately tuning $n_H$.

*j.zou@uq.edu.au
†z.chen1@uq.edu.au

 

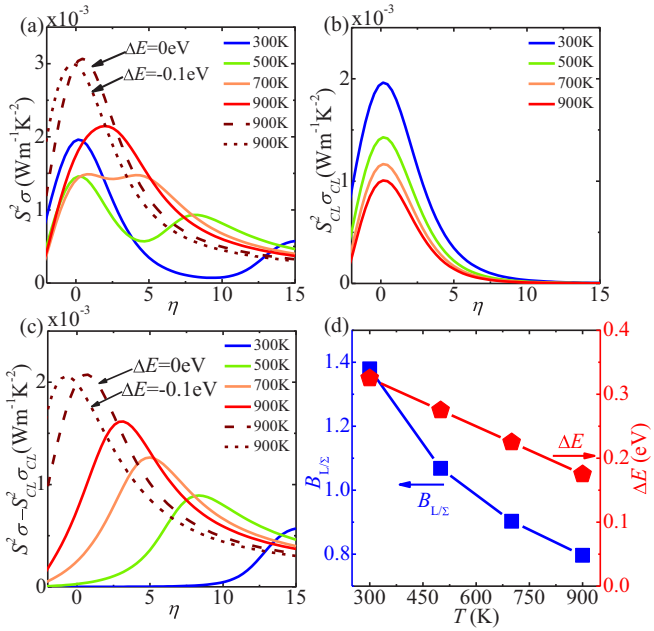


FIG. 1. Calculated (a) total power factor ($S^2\sigma$) using the three-band model to include the contributions of CB, $VB_L$, and, $VB_\Sigma$, (b) the partial power factor ($S^2_{CL}\sigma_{CL}$) using the two-band model to include the contributions of CB and $VB_L$, (c) and the partial power factor contributed by $VB_\Sigma$ ($S^2\sigma - S^2_{CL}\sigma_{CL}$), all as a function of reduced Fermi level ($\eta$) for SnTe at temperature ranging from 300 to 900 K. These three subfigures demonstrate the significant role of $VB_\Sigma$ in increasing the total $S^2\sigma$. (d) Temperature-dependent weighed mobility ratio between $VB_L$ and $VB_\Sigma$ ($B_{L/\Sigma}$) and energy separation between $VB_L$ and $VB_\Sigma$ ($\Delta E$) for SnTe. The variations of $B_{L/\Sigma}$ and $\Delta E$ interpret the increase of peak magnitude and the shift of peak for $S^2\sigma - S^2_{CL}\sigma_{CL}$ to low $\eta$ with increasing temperature being, respectively, caused by the decreased $B_{L/\Sigma}$ and $\Delta E$ at high temperature.

To quantitatively understand the contribution of $VB_\Sigma$ on thermoelectric properties, we used SnTe as an example. According to Eqs. (S1)–(S8) [28], for a given material at a certain temperature, its thermoelectric properties vary with $\eta$ [9,30,31]. Thus, we calculated the thermoelectric properties as a function of $\eta$ at a temperature range of 300–900 K. The calculated results are shown in the videos of the Supplemental Material [32], among which we highlighted $S^2\sigma$. It is noteworthy that the modeling here did not taking into account the possible additional carrier scatterings by various defects simultaneously introduced during engineering the band, or lowing the $\kappa_l$. If these do exist, the model might overestimate $S^2\sigma$ and $zT$ to some extent.

Figure 1(a) shows the temperature-dependent $S^2\sigma$ as a function of $\eta$, in which two peaks can be found at low temperature. With increasing $T$, they converge into one peak (e.g., $>$ 700 K) to achieve a higher $S^2\sigma$ of $\sim 2.1 \times 10^{-3}$ W m$^{-1}$ K$^{-2}$ at 900 K. In the calculations, we used $\Delta E = 0.45 - 2.5 \times 10^{-4} T$ [33], which means $\Delta E = 0.22$ eV at 900 K. Despite such an inherent temperature-dependent $\Delta E$, we calculated $S^2\sigma$ for $\Delta E = 0$ eV at 900 K and for $VB_\Sigma$ overtaking $VB_L$ to be the primary valance band (i.e., $\Delta E < 0$ eV). As can be seen, the peak $S^2\sigma$ increases to $\sim 3 \times 10^{-3}$ W m$^{-1}$ K$^{-2}$ for $\Delta E = 0$ eV at 900 K, while it decreases with further reducing $\Delta E$, for instance, to be $-0.1$ eV. Therefore, to maximize the peak $S^2\sigma$ in the situation of multibands, the band convergence should occur at the highest working temperature.

As a comparison, we calculated $S^2_{CL}\sigma_{CL}$ by only considering $VB_L$ and CB. Figure 1(b) shows the temperature-dependent $S^2_{CL}\sigma_{CL}$ as a function of $\eta$, in which the $S^2_{CL}\sigma_{CL}$ peaks stabilize at $\eta \approx 0.3$, in agreement with the previous study [31]. Moreover, the magnitude of the $S^2_{CL}\sigma_{CL}$ peak decreases with increasing $T$, due to (1) the stronger bipolar effect at high temperature (in turn reducing the thermoelectric performance); and (2) the increased effective mass for SnTe at high temperature [14], because large effective mass reduces $S^2_{CL}\sigma_{CL}$ [9].

Through subtracting $S^2_{CL}\sigma_{CL}$ from $S^2\sigma$, we can evaluate the contribution from $VB_\Sigma$. Figure 1(c) exhibits the derived $S^2\sigma - S^2_{CL}\sigma_{CL}$ as a function of $\eta$. With increasing $T$, the peak of $S^2\sigma - S^2_{CL}\sigma_{CL}$ shifts to low $\eta$, and the magnitude of the peak increases. To understand the variation of $S^2\sigma$, Fig. 1(d) plots the temperature-dependent weighted mobility ratio between $VB_L$ and $VB_\Sigma$ ($B_{L/\Sigma}$; refer to Eq. (S24) [28] for its calculation) and $\Delta E$, in which both $B_{L/\Sigma}$ and $\Delta E$ decrease with increasing $T$. According to the discussion in Sec. 3 of the Supplemental Material [28], decreasing $B_{L/\Sigma}$ and $\Delta E$ lead to an enhanced contribution from $VB_\Sigma$ in $S^2\sigma$ (corresponding to the increased peak magnitude of $S^2\sigma - S^2_{CL}\sigma_{CL}$ at high temperature). The shift of $S^2\sigma - S^2_{CL}\sigma_{CL}$ peak to low $\eta$ at high temperature is caused by the reduced $\Delta E$ (i.e., $VB_\Sigma$ moves close to $VB_L$).

In addition, the larger difference of peak positions between $S^2_{CL}\sigma_{CL}$ and $S^2\sigma - S^2_{CL}\sigma_{CL}$ at low temperature suggests that, at low temperature, $S^2\sigma$ is mainly contributed by CB + $VB_L$ (i.e., $S^2_{CL}\sigma_{CL}$) at low $\eta$, but is mainly contributed by $VB_\Sigma$ (i.e., $S^2\sigma - S^2_{CL}\sigma_{CL}$) at high $\eta$. From Fig. 1(a), for $T \leqslant 700$ K, $S^2\sigma$ has two peaks and the maximum value of $S^2\sigma$ corresponds to the peak at low $\eta$. Since the $S^2_{CL}\sigma_{CL}$ peak decreases with increasing $T$ [refer to Fig. 1(b)], the maximum value of $S^2\sigma$ at low $\eta$ decreases accordingly. With increasing $T$, the difference of peak positions between $S^2_{CL}\sigma_{CL}$ [refer to Fig. 1(b)] and $S^2\sigma - S^2_{CL}\sigma_{CL}$ [refer to Fig. 1(c)] becomes smaller, leading to the convergence of the two $S^2\sigma$ peaks at high temperature [refer to Fig. 1(a)]. Furthermore, with increasing $T$, the $S^2_{CL}\sigma_{CL}$ peak reduces while the $S^2\sigma - S^2_{CL}\sigma_{CL}$ peak increases, so that the contribution of $VB_\Sigma$ on $S^2\sigma$ becomes significant at high temperature.

In order to calculate $zT$, we should determine $\kappa$ first, including the components of $\kappa_l$,$\kappa_e$, and $\kappa_{bi}$ [34]. Herein, we calculated $\kappa_e$ and $\kappa_{bi}$ based on Eqs. (S7) and (S15), respectively, whereas $\kappa_l$ for SnTe was obtained from Ref. [14]. Figure 2(a) shows the calculated $\kappa_e$ as a function of $\eta$, in which $\kappa_e$ increases with increasing $T$ and $\eta$. This is because $\kappa_e$ is the thermal energy transported by free charger carriers [35]; high $T$ causes higher average thermal energy transported by an individual free charger carrier, resulting in a high $\kappa_e$. In addition, free charger carrier concentration increases with increasing $\eta$ [36], leading to high $\kappa_e$. Moreover, we also calculated $\kappa_e$ for $\Delta E = 0$ and $-0.1$ eV at 900 K, respectively. As can be seen, with decreasing $\Delta E$, $\kappa_e$ increases, which could partially offset the enhancement in $S^2\sigma$ caused by the decreased $\Delta E$.

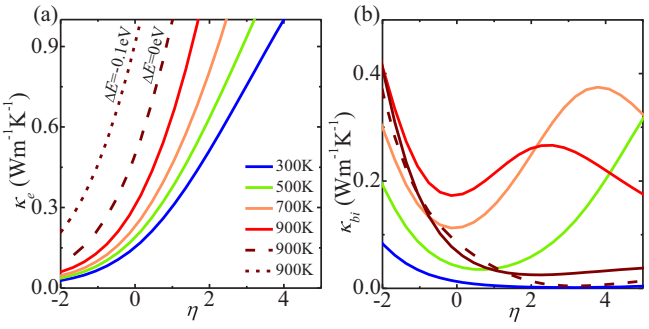


FIG. 2. Calculated (a) electronic thermal conductivity ($\kappa_e$), and (b) bipolar thermal conductivity ($\kappa_{bi}$) as a function of reduced Fermi level ($\eta$) for SnTe using the three-band model to include the contributions of CB, $VB_L$, and, $VB_\Sigma$ at temperature ranging from 300 to 900 K. These two subfigures present the effect of the energy separation between $VB_L$ and $VB_\Sigma$ ($\Delta E$) on $\kappa_e$ and $\kappa_{bi}$.

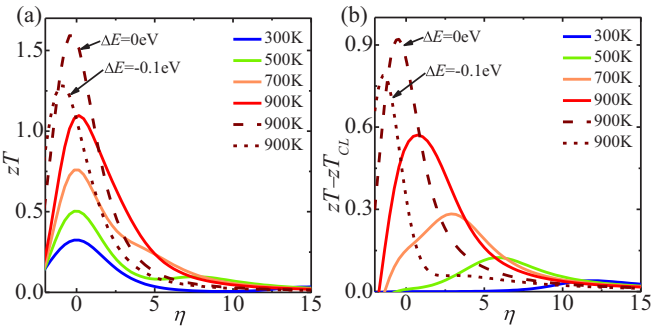


FIG. 3. Calculated (a) total figure of merit ($zT$) using the three-band model to include the contributions of CB, $VB_L$, and, $VB_\Sigma$, and (b) partial figure of merit contributed by $VB_\Sigma$ ($zT - zT_{CL}$) with $zT_{CL}$ denoting the partial figure of merit calculated using the two-band model to include the contributions of CB and $VB_L$, both $zT$ and $zT - zT_{CL}$ as a function of reduced Fermi level ($\eta$) for SnTe at temperature ranging from 300 to 900 K. These two subfigures illustrate the effect of reducing the energy separation between $VB_L$ and $VB_\Sigma$ ($\Delta E$) on increasing the total $zT$.

Figure 2(b) shows the calculated temperature-dependent $\kappa_{bi}$ as a function of $\eta$. Since $S^2\sigma$ reaches the peak value at 900 K and $\eta \approx 1$ [refer to Fig. 1(a)], we can examine the corresponding $\kappa_e$ and $\kappa_{bi}$ in this case. From Figs. 2(a) and 2(b), we found $\kappa_e \approx 0.5\,\mathrm{W\,m^{-1}\,K^{-1}}$ and $\kappa_{bi} \approx 0.2\,\mathrm{W\,m^{-1}\,K^{-1}}$ at 900 K and $\eta \approx 1$. Interestingly, in this case, $\kappa_{bi}$ is roughly 25% of $\kappa_e$, suggesting that $\kappa_{bi}$ plays an important role in determining the overall $zT$. Moreover, at 900 K, with reducing $\Delta E$ to 0 eV and even to $-0.1$ eV, $\kappa_{bi}$ was favorably decreased significantly; therefore band convergence can also suppress bipolar conduction.

By definition, $\kappa_{bi}$ is the thermal energy generated by the transition of electrons between different bands [34]. In the three-band case, $\kappa_{bi}$ includes three parts, i.e., electron transitions between CB and $VB_L$, between CB and $VB_\Sigma$, and between $VB_L$ and $VB_\Sigma$ [34]. To activate the contribution from $VB_\Sigma$, SnTe should be heavily doped, wherein electron transitions between CB and $VB_L$, and between CB and $VB_\Sigma$ are quite weak [37]. In this regard, $\kappa_{bi}$ is dominated by the electron transition between $VB_L$ and $VB_\Sigma$. For small $\Delta E$, the average thermal energy generated by the transition of electrons between $VB_L$ and $VB_\Sigma$ is low. Therefore, we can observe that $\kappa_{bi}$ decreases with reducing $\Delta E$ at 900 K.

Based on the calculated $S^2\sigma$, $\kappa_e$, $\kappa_{bi}$, and obtained $\kappa_l$, we calculated $zT$. Figure 3(a) shows the calculated $zT$ as a function of $\eta$ at temperature ranging between 300 and 900 K. As can be seen, different from the observed two peaks for $S^2\sigma$ in Fig. 3(a), $zT$ has only one peak at a given $T$, which is caused by the increased $\kappa_e$ and $\kappa_{bi}$ at large $\eta$. Moreover, with reducing $\Delta E$ to 0 eV at 900 K, $zT$ for SnTe is predicted to be 1.6, which means SnTe, the Pb-free rocksalt chalcogenide, is a promising candidate working at midtemperature range.

Figure 3(b) shows the temperature-dependent $zT - zT_{CL}$ as a function of $\eta$ to clarify the contribution of $VB_\Sigma$, in which $zT - zT_{CL}$ peaks increase with increasing $T$. At 900 K with the inherent $\Delta E$, the $zT$ peak reaches 1.2. Correspondingly, the $zT - zT_{CL} \approx 0.6$ can be obtained at 900 K from Fig. 3(b), indicating that nearly 50% of the peak $zT$ is contributed from $VB_\Sigma$. Moreover, for $\Delta E = 0$ eV at 900 K, the significantly increased peak $zT$ of 1.6 is caused by the increased $zT - zT_{CL}$. Therefore, we can conclude that the contribution of $VB_\Sigma$ is essential in enhancing the overall $zT$, particularly at high temperature.

So far, we have illustrated the thermoelectric properties as a function of $\eta$ for SnTe, which describes how band structure affects the electronic transport, and we found that $zT$ for SnTe reaches up to 1.6 for $\Delta E = 0$ eV at 900 K. Following this, we predicted the maximum $zT$ in both PbTe and PbSe. To achieve the maximum $zT$, one condition is to produce the convergence of $VB_L$ and $VB_\Sigma$ at the highest working temperature, and the other is to properly tune $n_H$. As such, it is necessary to determine the corresponding $n_H^{opt}$ for these rocksalt structured chalcogenides. To this end, we calculated the thermoelectric properties as functions of $T$ and $n_H$ for SnTe, PbTe, and PbSe with band convergence occurring at 900 K, shown in Figs. S2–S4 (see Ref. [28]). The feasibility of our calculations was verified via comparing our calculated $S$, $\mu_H$, $S^2\sigma$, and $zT$ as a function of $n_H$ with the reported experimental values of Na-doped PbSe [10], Na-doped PbTe [29], and I-doped SnTe [14]. All the comparisons are shown in Figs. S5–S7 (see Ref. [28]), in which experimental values can coincide with our calculated curves of $S$, $\mu_H$, $S^2\sigma$, and $zT$ (from CB + $VB_L$ + $VB_\Sigma$) at a wide temperature range, confirming the feasibility of our calculations.

On this basis, we determined the $n_H^{opt}$ for $S^2\sigma$, and for $zT$, shown in Figs. 4(a) and 4(b), respectively. As can be seen, $n_H^{opt}$ for $zT$ is lower than that for $S^2\sigma$, which is to compromise the increased $\kappa_e$ at large $n_H$ (i.e., large $\eta$). Moreover, we calculated the temperature-dependent $S^2\sigma$ and $zT$ for some typical $n_H$ values. Figure 4(c) shows the temperature-dependent $S^2\sigma$, in which the dash curves correspond to $n_H = n_H^{opt}$ for $S^2\sigma$ at 900 K, and the solid curves correspond to $n_H = n_H^{opt}$ for $zT$ at 900 K. As can be seen, the solid curves are lower than the corresponding dash curves, which means at $n_H^{opt}$ for maximizing $zT$, the corresponding $S^2\sigma$ is not maximized. Figure 4(d) shows the temperature-dependent $zT$ (solid curves) for $n_H$ equaling the 900 K $n_H^{opt}$ with the reported $\kappa_l$ from Ref. [29] for PbTe, Ref. [10] for PbSe, and Ref. [14] for SnTe. As can be seen, the maximum $zT$ values for PbTe, PbSe,

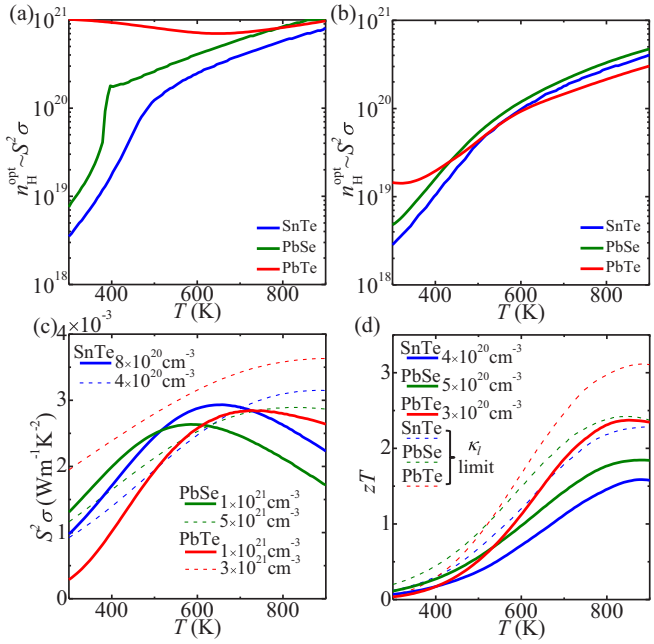


FIG. 4. Determined temperature-dependent optimal Hall carrier concentration ($n_H^{opt}$) for (a) total power factor ($S^2\sigma$) and (b) total figure of merit ($zT$) using the three-band model. (c) Calculated total power factor ($S^2\sigma$) and (d) total figure of merit ($zT$) using the three-band model as a function of temperature for SnTe, PbSe, and PbTe, respectively. These figures demonstrate the significant enhancement in $zT$ by only reducing the energy separation between $VB_L$ and $VB_\Sigma$ ($\Delta E$), and the further enhancement in $zT$ by reducing the lattice thermal conductivity ($\kappa_l$) to the amorphous limits of these rocksalt structured materials.

and SnTe are predicted to be 2.2, 1.8, and 1.6. In addition, if we used the amorphous limit $\kappa_l$ of 0.36 W m$^{-1}$ K$^{-1}$ for PbTe [38], of 0.35 W m$^{-1}$ K$^{-1}$ of for PbSe [39], and of 0.4 W m$^{-1}$ K$^{-1}$ for SnTe [40], the maximum $zT$ could be further enhanced to 3.1, 2.4, and 2.2, respectively. It should be noted that increasing $n_H$ to $n_H^{opt}$ by doping might induce the ionized impurity scattering to some extent. To clarify the impact of the ionized impurity scattering, we compared the thermoelectric properties in the cases of considering acoustic phonon scattering only and considering both acoustic phonon and ionic impurity scatterings. Figure S8 shows the comparison (see Ref. [28]), from which the coexistence of acoustic phonon and ionic impurity scatterings leads to slight decreases in both $S^2\sigma$ and $zT$. In particular, the $zT$ reduction is $< 1\%$.

In this study, we performed simulations based on the three-model for SnTe as an example. Qualitatively, we found that accompanying the enhancement in $S^2\sigma$ caused by $VB_\Sigma$, $\kappa_e$ is also increased. Such an increase in $\kappa$ can partially offset the enhancement in $S^2\sigma$ caused by $VB_\Sigma$ for the overall $zT$. Moreover, we determined the $n_H^{opt}$ for $S^2\sigma$ and $zT$ in PbTe, PbSe, and SnTe, which suggests that highly doped $p$-type rocksalt structured chalcogenides are required for maximizing the thermoelectric efficiency. Combining the reported $\kappa_l$ from the literature, we predicted the maximum $zT$ values for PbTe, PbSe, and SnTe can be 2.2, 1.8, and 1.6, respectively. If $\kappa_l$ reaches the amorphous limit, $zT$ could be further enhanced to 3.1, 2.4, and 2.2, respectively. This study suggests that there is plenty of room for $zT$ improvement in the currently reported PbTe, PbSe, and SnTe when producing the band convergence at 900 K with properly tuned $n_H$.

This work was financially supported by the Australian Research Council. M.H. thanks the China Scholarship Council for providing the Ph.D. stipend, and the Graduate School of the University of Queensland for providing the travel award.

[1] L. E. Bell, Science **321**, 1457 (2008).
[2] Z.-G. Chen, G. Han, L. Yang, L. Cheng, and J. Zou, Prog. Nat. Sci. **22**, 535 (2012).
[3] M. Hong, T. C. Chasapis, Z.-G. Chen, L. Yang, M. G. Kanatzidis, G. J. Snyder, and J. Zou, ACS Nano **10**, 4719 (2016).
[4] Y. Pei, H. Wang, and G. J. Snyder, Adv. Mater. **24**, 6125 (2012).
[5] S. Lin, W. Li, Z. Chen, J. Shen, B. Ge, and Y. Pei, Nat. Commun. **7**, 10287 (2016).
[6] L.-D. Zhao, G. Tan, S. Hao, J. He, Y. Pei, H. Chi, H. Wang, S. Gong, H. Xu, V. P. Dravid, C. Uher, G. J. Snyder, C. Wolverton, and M. G. Kanatzidis, Science **351**, 141 (2016).
[7] L.-D. Zhao, V. P. Dravid, and M. G. Kanatzidis, Energy Environ. Sci. **7**, 251 (2014).
[8] S. I. Kim, K. H. Lee, H. A. Mun, H. S. Kim, S. W. Hwang, J. W. Roh, D. J. Yang, W. H. Shin, X. S. Li, Y. H. Lee, G. J. Snyder, and S. W. Kim, Science **348**, 109 (2015).
[9] Y. Pei, A. D. LaLonde, H. Wang, and G. J. Snyder, Energy Environ. Sci. **5**, 7963 (2012).
[10] H. Wang, Y. Pei, A. D. LaLonde, and G. J. Snyder, Adv. Mater. **23**, 1366 (2011).
[11] T. C. Chasapis, Y. Lee, E. Hatzikraniotis, K. M. Paraskevopoulos, H. Chi, C. Uher, and M. G. Kanatzidis, Phys. Rev. B **91**, 085207 (2015).
[12] G. Tan, F. Shi, J. W. Doak, H. Sun, L.-D. Zhao, P. Wang, C. Uher, C. Wolverton, V. P. Dravid, and M. G. Kanatzidis, Energy Environ. Sci. **8**, 267 (2015).
[13] Y. Pei, H. Wang, Z. M. Gibbs, A. D. LaLonde, and G. J. Snyder, NPG Asia Mater. **4**, e28 (2012).
[14] M. Zhou, Z. M. Gibbs, H. Wang, Y. Han, C. Xin, L. Li, and G. J. Snyder, Phys. Chem. Chem. Phys. **16**, 20741 (2014).
[15] M. Hong, Z.-G. Chen, L. Yang, G. Han, and J. Zou, Adv. Electron. Mater. **1**, 1500025 (2015).
[16] B. L. Huang and M. Kaviany, Phys. Rev. B **77**, 125209 (2008).
[17] S. V. Faleev and F. Léonard, Phys. Rev. B **77**, 214304 (2008).
[18] Z. M. Gibbs, H. Kim, H. Wang, R. L. White, F. Drymiotis, M. Kaviany, and G. J. Snyder, Appl. Phys. Lett. **103**, 262109 (2013).
[19] Y. Pei, X. Shi, A. LaLonde, H. Wang, L. Chen, and G. J. Snyder, Nature **473**, 66 (2011).
[20] Q. Zhang, F. Cao, W. Liu, K. Lukas, B. Yu, S. Chen, C. Opeil, D. Broido, G. Chen, and Z. Ren, J. Am. Chem. Soc. **134**, 10031 (2012).
[21] H. Wang, Z. M. Gibbs, Y. Takagiwa, and G. J. Snyder, Energy Environ. Sci. **7**, 804 (2014).

[22] W. Li, Z. Chen, S. Lin, Y. Chang, B. Ge, Y. Chen, and Y. Pei, J. Materiomics **1**, 307 (2015).

[23] G. Tan, F. Shi, S. Hao, H. Chi, T. P. Bailey, L.-D. Zhao, C. Uher, C. Wolverton, V. P. Dravid, and M. G. Kanatzidis, J. Am. Chem. Soc. **137**, 11507 (2015).

[24] G. Tan, L.-D. Zhao, F. Shi, J. W. Doak, S.-H. Lo, H. Sun, C. Wolverton, V. P. Dravid, C. Uher, and M. G. Kanatzidis, J. Am. Chem. Soc. **136**, 7006 (2014).

[25] G. Tan, F. Shi, S. Hao, H. Chi, L.-D. Zhao, C. Uher, C. Wolverton, V. P. Dravid, and M. G. Kanatzidis, J. Am. Chem. Soc. **137**, 5100 (2015).

[26] L. D. Zhao, H. J. Wu, S. Q. Hao, C. I. Wu, X. Y. Zhou, K. Biswas, J. Q. He, T. P. Hogan, C. Uher, C. Wolverton, V. P. Dravid, and M. G. Kanatzidis, Energy Environ. Sci. **6**, 3346 (2013).

[27] G. S. Nolas, J. Sharp, and H. J. Goldsmid, *Thermoelectrics: Basic* (Springer, Berlin, 2001).

[28] See Supplemental Material at http://link.aps.org/supplemental/10.1103/PhysRevB.94.161201 for details of modeling process, mathematical clarification, calculation of weighted mobility ratio, determination of optimal carrier concentration, comparision of calculated curves with reported data, and examination of impurity scattering.

[29] Y. Pei, A. LaLonde, S. Iwanaga, and G. J. Snyder, Energy Environ. Sci. **4**, 2085 (2011).

[30] Y. I. Ravich, B. A. Efimova, and I. A. Smirnov, *Semiconducting Lead Chalcogenides* (Plenum Press, New York, 1970).

[31] Y. Pei, Z. M. Gibbs, B. Balke, W. G. Zeier, and G. J. Snyder, Adv. Energy Mater. **4**, 1400486 (2014).

[32] See Supplemental Material at http://link.aps.org/supplemental/10.1103/PhysRevB.94.161201 for videos showing the calculated thermoelectric properties as a function of reduced Fermi level at 300–900 K.

[33] L. M. Rogers, J. Phys. D: Appl. Phys. **1**, 845 (1968).

[34] L. Zhang, P. Xiao, L. Shi, G. Henkelman, J. B. Goodenough, and J. Zhou, J. Appl. Phys. **117**, 155103 (2015).

[35] A. J. Minnich, M. S. Dresselhaus, Z. F. Ren, and G. Chen, Energy Environ. Sci. **2**, 466 (2009).

[36] P. Pichanusakorn and P. Bandaru, Mater. Sci. Eng., R **67**, 19 (2010).

[37] S. Wang, J. Yang, T. Toll, J. Yang, W. Zhang, and X. Tang, Sci. Rep. **5**, 10136 (2015).

[38] Y. Pei, J. Lensch-Falk, E. S. Toberer, D. L. Medlin, and G. J. Snyder, Adv. Funct. Mater. **21**, 241 (2011).

[39] Q. Zhang, E. K. Chere, K. McEnaney, M. Yao, F. Cao, Y. Ni, S. Chen, C. Opeil, G. Chen, and Z. Ren, Adv. Energy Mater. **5**, 1401977 (2015).

[40] Y. Pei, L. Zheng, W. Li, S. Lin, Z. Chen, Y. Wang, X. Xu, H. Yu, Y. Chen, and B. Ge, Adv. Electron. Mater. **2**, 1600019 (2016).